I&EC research
Industrial & Engineering Chemistry Research

Article

pubs.acs.org/IECR

Nonintrusive Uncertainty Quantification of Computational Fluid Dynamics Simulations of a Bench-Scale Fluidized-Bed Gasifier

Aytekin Gel,*[,†,‡] Mehrdad Shahnam,[†] Jordan Musser,[†] Arun K. Subramaniyan,[§] and Jean-François Dietiker[†,⊥]

[†]National Energy Technology Laboratory (NETL), Morgantown, West Virginia 26505, United States
[‡]ALPEMI Consulting, LLC, Phoenix, Arizona 85044, United States
[§]General Electric (GE) Global Research Center, Niskayuna, New York 12309, United States
[⊥]West Virginia University Research Corporation, Morgantown, West Virginia 26505, United States

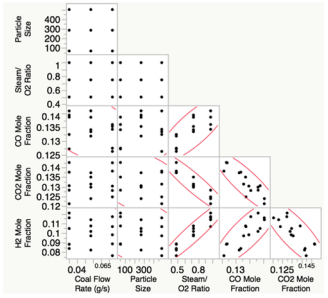

Scatterplot matrix of input and output from MFIX sampling simulation runs

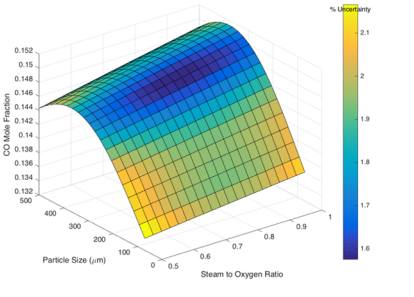

Surrogate model (Emulator) constructed from MFIX sampling simulation output (CO mole fraction)

ABSTRACT: Uncertainty quantification (UQ) analysis is increasingly becoming one of the major requirements of simulation-based engineering to assess the confidence in the results and make better-informed decisions based on the insight derived from the simulations. In an earlier study, Bayesian UQ analysis was applied to existing bench-scale fluidized-bed gasifier experiment results. In the current study, a series of simulations were carried over with the open-source computational fluid dynamics software MFiX to reproduce the experimental conditions, where three operating factors, i.e., coal flow rate, coal particle diameter, and steam-to-oxygen ratio, were systematically varied to understand their effect on the syngas composition. Bayesian UQ analysis was this time performed on the numerical results for comparison purposes. This is part of ongoing research efforts to explore the applicability of advanced UQ methods and processes such as Bayesian methods for large-scale complex multiphase flow simulations. As part of Bayesian UQ analysis, a global sensitivity analysis was performed based on the simulation results, which shows that the predicted syngas composition is strongly affected not only by the steam-to-oxygen ratio (which was observed in experiments as well) but also by variation in the coal flow rate and particle diameter (which was not observed in experiments). The carbon monoxide mole fraction is underpredicted at lower steam-to-oxygen ratios and overpredicted at higher steam-to-oxygen ratios. The opposite trend is observed for the carbon dioxide mole fraction. These discrepancies are attributed to either excessive segregation of the phases that leads to the fuel-rich or -lean regions or alternatively the selection of reaction models, where different reaction models and kinetics can lead to different syngas compositions throughout the gasifier.

INTRODUCTION

The application of scientific computer simulations to the design of complex engineering systems, ranging from aerospace vehicles to automobile engines, has dramatically increased in recent years. This has reduced the number of physical models or prototypes that need to be built, resulting in significant savings in the cost and time required to get the products to market. Such an acceleration of technology development is of practical relevance to energy systems because global changes in ecosystems and climate require the accelerated development of new advanced technologies for the clean and efficient utilization of coal, renewable energy, and carbon capture and storage. Process simulation is now routinely used for the analysis and design of energy systems, and computational fluid dynamics (CFD) has become a valuable tool to design and troubleshoot energy conversion devices. To achieve the goal of using simulations to reduce the time required to take energy technologies from discovery to commercial deployment, the simulations must reliably predict the performance of scaled-up devices that are under design as well as devices at scales that have not been built or tested. It is not possible to predict the performance of such complex systems with 100% certainty, and

Received: June 30, 2016
Revised: September 29, 2016
Accepted: October 20, 2016
Published: October 20, 2016

DOI: 10.1021/acs.iecr.6b02506
Ind. Eng. Chem. Res. XXXX, XXX, XXX−XXX

it will be essential to quantify the uncertainty in the predictions to make appropriate design decisions.

In this study, we assess the feasibility of employing Bayesian uncertainty quantification (UQ) methods in a chemically reacting multiphase CFD simulation, which is used for the design of energy conversion devices. In multiphase CFD simulations, usually the level of uncertainty is currently not quantified and is characterized only by the qualitative assessment of the discrepancy observed during validation studies. The lack of quantified uncertainty diminishes the confidence with which multiphase CFD modeling and simulations can be used for making design decisions. Furthermore, the lack of quantified uncertainty reduces the ability to identify areas of model improvement required to increase confidence in the simulation results. The present paper originates from an effort underway at the National Energy Technology Laboratory (NETL) of the U.S. Department of Energy (DOE) to quantify the uncertainty in multiphase CFD models to help overcome these deficiencies. In our earlier studies,[1,2] traditional UQ methods such as the comprehensive UQ framework developed by Roy and Oberkampf[3] were applied to nonreacting multiphase flows in a riser.

On the basis of the insight gained from earlier work, this study aims to explore the applicability of more sophisticated UQ methods such as Bayesian UQ analysis for more complex reacting multiphase flows such as those in fluidized-bed gasifiers. Hence, the objectives of this paper are to outline a general UQ methodology and demonstrate its applicability to real-life engineering problems through a representative demonstration problem. For this purpose, a bench-scale fluidized-bed gasifier with experimental data has been simulated by replicating the physical experiments, which were originally designed through the use of a statistical design of experiments methods. Hence, these experiments were unique in a way that adequate data for carrying out UQ analysis were available.

The paper has been organized as follows: we first briefly introduce the theory of the Bayesian UQ methodology applied. The demonstration problem selected for this study with the experimental data and computational modeling approach employed is introduced next. A brief discussion on the application of the proposed UQ methodology to the standalone experimental results is presented, which was not performed by the authors of the original study. A more detailed study utilizing only the experimental observations and associated data was carried out in work by Gel et al.,[4] which the current paper builds upon. Hence, the contribution of the paper is the extension and demonstration of the application of Bayesian hybrid UQ methods to the existing experimental data and CFD simulations with the open-source CFD code MFiX, which are presented in the following section. Some of the initial observations and insights, which have motivated the follow-up studies,[22] are reported in the Conclusions section.

BAYESIAN UQ ANALYSIS METHOD

Kennedy and O'Hagan[5] proposed a Bayesian framework to combine the experimental data and high-fidelity simulations. In this framework, the simulation model output is approximated using a Gaussian process model (GPM), and the hyperparameters of the GPM are calibrated through a Markov chain Monte Carlo procedure to obtain the posterior distributions of the hyperparameters. The calibrated GPMs can then be used to make predictions at a given input configuration. This framework was implemented by researchers at Los Alamos National Laboratory of the U.S. DOE in their GPMs for simulation analysis code. In this paper, a modified version (by GE) of Kennedy and O'Hagan's Bayesian Hybrid Modeling framework is used, which will be referred to as GEBHM analysis in the rest of the paper.

The physics-based CFD model is considered to be inherently not accurate, and the potential discrepancy is modeled as a separate model. Overtuning of the model parameters is avoided by simultaneously calibrating the parameters and computing the model discrepancy.

These techniques have been successfully applied on GE applications for calibrating complex nonlinear systems under uncertain conditions. The methodology has been documented in detail, and the interested reader can refer to work by Subramaniyan et al.[6,7] and Kumar et al.[8]

BENCH-SCALE FLUIDIZED-BED GASIFIER EXPERIMENTS

Gasification is one of the promising power-generation technologies that can offer high efficiency while keeping pollutants at lower levels than the typical combustion-based technologies. A key feature of the gasification process is the extraction of carbon from diverse feedstocks through a chemical reaction process to produce synthetic natural gas (syngas). A number of initiatives at the NETL aim to develop and improve advanced gasification technologies. Hence, employing an integrated framework that combines theoretical and experimental research with credible predictive models plays an important role. As part of this effort, a bench-scale fluidized-bed gasifier studied by Karimipour et al.,[9] which is shown in Figure 1, was modeled, and the CFD simulation results were compared against the experimental results for the gasifier with the same configuration and operating conditions. In the same study, a series of gasification experiments were performed (see Table 1) to approximately characterize the effect of the coal feed rate (referred to as factor 1, which was varied between 0.036 and 0.063 g/s), coal particle size (factor 2 varied between

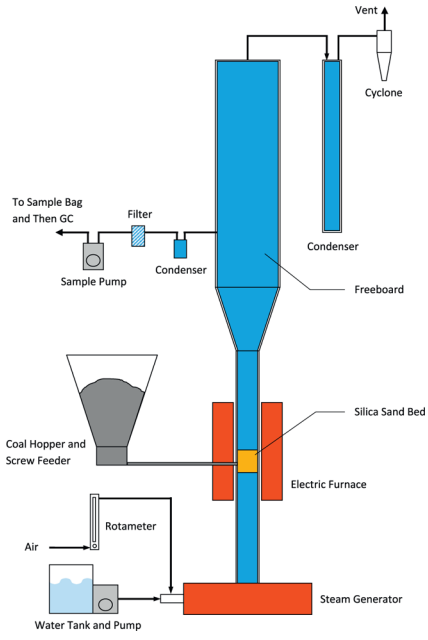

Figure 1. Schematic illustration of the bench-scale fluidized-bed gasifier used in the study of Karimipour et al.[9]

DOI: 10.1021/acs.iecr.6b02506
Ind. Eng. Chem. Res. XXXX, XXX, XXX−XXX

Table 1. Tabulated Data for Input and All QoIs (response) from the Experiments[9]

	uncertain input parameters/factors			QoIs or response variables					secondary QoIs (acquired via personal communication[10])				
	factor 1	factor 2	factor 3	response 1	response 2	response 3	response 4	response 5	response 6	response 7	response 8	response 9	response 10
actual experiment run order	coal flow rate (g/s)	particle size (μm)	H_2O/O_2 ratio in syngas	carbon conversion (%)	H_2/CO ratio in syngas	CH_4/H_2 ratio in syngas	gasification efficiency (%)	gas yield (m^3/kg of coal)	CH_4 mole fraction	CO mole fraction	CO_2 mole fraction	H_2 mole fraction	N_2 mole fraction
1	0.063	70	0.5	91.57	0.81	0.0646	56.50	3.45	0.007	0.143	0.131	0.115	0.579
2	0.063	70	1	93.35	1.249	0.0517	57.92	3.57	0.007	0.111	0.156	0.139	0.559
3	0.0495	70	0.75	92.56	1.048	0.0573	59.03	3.47	0.008	0.130	0.143	0.135	0.558
4	0.036	70	0.5	92.26	0.816	0.0662	59.83	3.42	0.008	0.150	0.126	0.122	0.568
5	0.036	70	1	93.61	1.23	0.0519	61.17	3.54	0.008	0.122	0.149	0.151	0.543
6	0.063	285	0.75	96.59	1.037	0.0579	62.24	3.63	0.008	0.132	0.139	0.135	0.559
7	0.0495	285	0.5	93.79	0.81	0.0654	63.93	3.5	0.008	0.145	0.130	0.117	0.575
8	0.0495	285	0.75	95.48	1.006	0.0587	62.12	3.57	0.008	0.136	0.138	0.135	0.556
9	0.0495	285	0.75	96	1.011	0.0574	62.24	3.61	0.008	0.136	0.138	0.136	0.556
10	0.0495	285	0.75	96	0.987	0.0582	60.79	3.6	0.008	0.133	0.140	0.133	0.560
11	0.0495	285	0.75	96	0.975	0.057	66.88	3.65	0.008	0.141	0.135	0.143	0.545
12	0.0495	285	0.75	96.89	1.003	0.0587	64.07	3.66	0.008	0.135	0.138	0.137	0.555
13	0.0495	285	0.75	96.42	1.01	0.0586	63.66	3.65	0.008	0.135	0.138	0.134	0.559
14	0.0495	285	1	95.41	1.215	0.0528	59.50	3.63	0.007	0.114	0.153	0.139	0.559
15	0.036	285	0.75	95.68	1.013	0.0574	61.37	3.59	0.008	0.132	0.139	0.135	0.559
16	0.063	500	0.5	91.1	0.812	0.0674	56.23	3.44	0.008	0.139	0.133	0.117	0.578
17	0.063	500	1	94.33	1.268	0.0537	58.98	3.6	0.008	0.112	0.156	0.142	0.556
18	0.0495	500	0.75	93.83	1.017	0.0611	58.84	3.56	0.008	0.127	0.144	0.130	0.566
19	0.036	500	0.5	93.58	0.776	0.0702	59.42	3.47	0.008	0.150	0.126	0.114	0.577
20	0.036	500	1	96.41	1.186	0.0553	62.94	3.63	0.008	0.124	0.149	0.150	0.542

DOI: 10.1021/acs.iecr.6b02506
Ind. Eng. Chem. Res. XXXX, XXX, XXX−XXX

70 and 500 μm), and steam-to-oxygen ratio (factor 3 varied between 0.5 and 1.0) on the quality of syngas generated. The response variables or quantities of interest (QoIs) were carbon conversion (%), hydrogen (H_2)/carbon monoxide (CO) and methane (CH_4)/H_2 ratios in syngas, gasification efficiency (%), and gas yield (m^3/kg). Hence, in the original study, within the primary QoI variables, the species mole fractions were only reported as a ratio such as H_2/CO. For the purposes of this study, mole fractions measured at the monitoring location in the experiments were obtained from the authors[10] and considered as the targeted QoIs to perform GEBHM analysis.

The study of Karimipour et al.[9] was selected because of several unique features, such as the way in which the physical experiments were designed and executed. The experimental conditions were determined through the statistical design of experiments technique where 15 distinct experimental conditions were tested by varying factors 1−3, with one experimental condition being replicated six times, so a total of 20 samples of experimental data were generated, as shown in Table 1. However, some of the fundamental requirements of the statistical design of experiments were not completely followed such as randomization and replication of all samples to increase confidence in the experimental measurements. In our study, the available replications of the same run conditions were useful in assessing and estimating the experimental errors. A central composite design (CCD) based statistical design of experiments technique[11] was utilized by Karimipour et al.[9] Additionally, a response surface methodology[11] was used to investigate the effect of the independent variables (coal feed rate, coal particle size, and steam-to-oxygen ratio) on the response variables, such as the syngas quality as characterized by the H_2/CO and CH_4/H_2 ratios.

The results of the physical experiments performed in the study of Karimipour et al.[9] are summarized in Table 1. The replication runs, which were performed for the center point, are between 8 and 13 (which are in bold italics in the "actual experiment run order" column). In addition to the experiments performed based on CCD-based sampling runs, four additional experiments were conducted for validation purposes.

A preliminary UQ analysis was performed by employing the GEBHM approach for the experimental results shown in Table 1, which was not performed in the original study, and is presented in the remainder of the paper.

Bayesian UQ Analysis of the Experimental Results. In the study of Karimipour et al.,[9] a preliminary analysis of the data acquired from experiments was performed using the analysis of variance (ANOVA) method.[11] In addition, response surfaces based on regression employing second-order polynomials (Table 4 in the original paper[9]) were generated to relate the primary QoIs with the three operating variables. For example, a functional relationship was established between the gasification efficiency and the three operating variables (coal flow rate, coal particle size, and steam-to-oxygen ratio). However, the original study did not include any systematic UQ analysis in spite of the extensive experimental data collected. In a recent study,[4] we employed a Bayesian UQ analysis method, i.e., GEBHM, which was introduced briefly in section 2, to analyze the results obtained from experiments before proceeding with the extension of the same methodology to CFD simulation results, which is the primary focus of the current paper. A different set of QoIs was employed, i.e., instead of the derived or ratio-based quantities used in the original study,[9] direct field variables for species mole fractions [CO, carbon dioxide (CO_2), and H_2] were used after the experimental raw data were acquired through a personal communication with the original authors. In the initial Bayesian UQ study with an experimental data set,[4] a GPM-based emulator (or a surrogate model) was constructed from the CCD-based 20 samples obtained with physical experiments. A global sensitivity study was conducted to understand which operating variables have the most effect on the QoIs. Table 2

Table 2. Global Sensitivity of the QoIs with Respect to the Operating Variables in the Original Experiments of Karimipour et al.[9] with CCD Sampling

% Contribution to the Variability Seen in the CO Mole Fraction			
	factor 1	factor 2	factor 3
	CF	PS	H_2O/O_2
CF: coal flow rate (g/s)	1.6	0.05	1.1
PS: particle size (μm)		0.2	0.1
H_2O/O_2 ratio in syngas			**96.9**
% Contribution to the Variability Seen in the H_2 Mole Fraction			
	factor 1	factor 2	factor 3
	CF	PS	H_2O/O_2
CF: coal flow rate (g/s)	0.9	0.32	1.7
PS: particle size (μm)		1.4	0.4
H_2O/O_2 ratio in syngas			**95.3**
% Contribution to the Variability Seen in the CO_2 Mole Fraction			
	factor 1	factor 2	factor 3
	CF	PS	H_2O/O_2
CF: coal flow rate (g/s)	1.0	0.01	0.6
PS: particle size (μm)		0.1	0.1
H_2O/O_2 ratio in syngas			**98.3**

shows the results of the global sensitivity analysis by applying GEBHM to the experimental results only. The application of GEBHM analysis for the experimental data clearly shows that the steam-to-oxygen ratio has the most pronounced effect on all QoIs under consideration. Also, an analysis was carried out for the forward propagation of uncertainties in operating variables and procedure to determine the next set of best sampling candidates if we were to conduct additional experiments.

Figure 2 shows the variance in the global sensitivity for each QoI, which is generated as part of GEBHM analysis. These plots show the overall sensitivity of each operating variable to the corresponding QoI. The median of the sensitivity is shown as a darker horizontal line in the middle of the box plot. A sensitivity value close to zero indicates low sensitivity, and that close to one indicates very high sensitivity.[12] For example, for all QoIs under consideration, the steam-to-oxygen ratio is identified as the most sensitive parameter. However, because the variance in the sensitivity for this parameter ranges from 0 to 1, the sensitivity varies significantly depending on the location in the parameter design space; i.e., depending on where the other two variables are set, the steam ratio could be very sensitive or completely insensitive. Hence, although the coal flow rate and particle size do not affect the syngas composition directly, they are still very important because they influence the steam-to-oxygen ratio, which is the most sensitive parameter. Additional details on the Bayesian UQ analysis of the experimental data and results can be found in the work by Gel et al.[4]

DOI: 10.1021/acs.iecr.6b02506
Ind. Eng. Chem. Res. XXXX, XXX, XXX−XXX

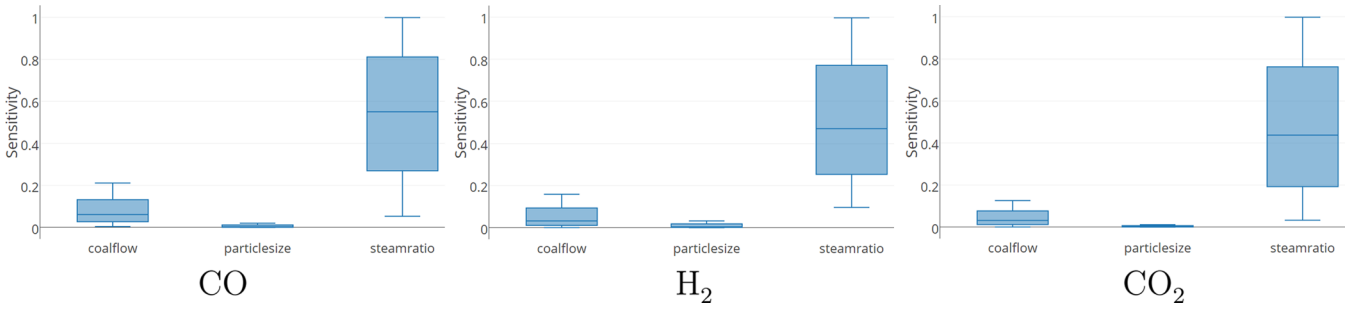

Figure 2. Variance of the global sensitivity for each QoI based on the experiment data.

CFD MODEL AND SIMULATIONS

MFiX,[13] which is an open-source CFD software suite developed and maintained by the U.S. DOE's NETL, was used to model the bench-scale fluidized-bed gasifier studied by Karimipour et al.[9] MFiX is a suite of CFD solvers that includes both continuum (multifluid) and discrete (DEM and MP-PIC) approaches to multiphase-flow modeling (such as gas−solid flows typically encountered in a fluidized bed). In this study, the multifluid framework in MFiX [i.e., MFiX two-fluid model (MFiX-TFM) solver's 2015-2 release version] has been used. Hence, the gaseous mixture is modeled as a gas phase, and the particulates are modeled as an interpenetrating continuous solid phase. Multiple solid phases can be used to describe multiple particulate materials. In this work, two distinct solid phases are used to describe coal and sand particles. The governing equations employed for the conservation of mass, momentum, energy, and species transport for each phase (m = g for gas and m = s for solid) are

$$\frac{\partial}{\partial t}(\varepsilon_m \rho_m) + \nabla\cdot(\varepsilon_m \rho_m \vec{v}_m) = \sum_{n=1}^{N_m} R_{mn} \tag{1}$$

$$\frac{\partial}{\partial t}(\varepsilon_m \rho_m \vec{v}_m) + \nabla\cdot(\varepsilon_m \rho_m \vec{v}_m \vec{v}_m) = \nabla\cdot\bar{\bar{S}}_m + \varepsilon_m \rho_m \vec{g} + \sum_n \vec{I}_{mn} \tag{2}$$

$$\varepsilon_m \rho_m C_{pm}\left(\frac{\partial T_m}{\partial t} + \vec{v}_m\cdot\nabla T_m\right) = -\nabla\cdot\vec{q}_m + \sum_n \gamma_{mn}(T_n - T_m) - \Delta H_{rm} \tag{3}$$

$$\frac{\partial}{\partial t}(\varepsilon_m \rho_m X_{ml}) + \nabla\cdot(\varepsilon_m \rho_m X_{ml} \vec{v}_m) = R_{ml} \tag{4}$$

where subscripts m and n represent phases and l represents a species in a phase. The closure terms for the solid phases are obtained through kinetic granular theory with an algebraic form of the granular temperature equation. The Schaeffer frictional model was used in the dense regions, and Gunn's correlation was used for heat transfer. The momentum transfer between the gas and solid phases is modeled using the Gidaspow drag model in MFiX-TFM. Detailed information on the constitutive relationships used to model the momentum and energy exchange terms between the phases along with the solid stress model used in MFiX can be obtained in MFiX online documentation.[14,15] The complex chemical processes taking place in the gasifier are modeled using the following single-step heterogeneous and homogeneous reaction mechanisms, which utilized the stiff solver developed for MFiX-TFM.

Heterogeneous Reactions

Coal Moisture Release:

$$H_2O(l) \rightarrow H_2O(g) \tag{5}$$

Devolatization:

$$\text{coal } (CH_mO_n)(s) \rightarrow (n_{CO_2})CO_2 + (n_{CO})CO + (n_{H_2})H_2 + (n_{CH_4})CH_4 + (n_{H_2O})H_2O + (n_{H_2S})H_2S + (n_{C_3H_6})C_3H_6 + (n_{HCN})HCN + (n_{C_2H_4})C_2H_4 + (n_{C_2H_6})C_2H_6 \tag{6}$$

Char Oxidation:

$$C + \frac{1}{2}O \rightarrow CO \tag{7}$$

Steam Gasification:

$$C + H_2O \rightarrow CO + H_2 \tag{8}$$

CO_2 Gasification:

$$C + CO_2 \rightarrow 2CO \tag{9}$$

Catalytic Water−Gas Shift (WGS):

$$CO + H_2O \leftrightarrow CO_2 + H_2 \tag{10}$$

Homogeneous Reactions

CO Oxidation:

$$CO + \frac{1}{2}O_2 \rightarrow CO_2 \tag{11}$$

H_2 Oxidation:

$$2H_2 + O_2 \rightarrow 2H_2O \tag{12}$$

Methane Oxidation:

$$CH_4 + 2O_2 \rightarrow CO_2 + 2H_2O \tag{13}$$

where (g), (l), and (s) denote gas, liquid, and solid phases, respectively.

The reaction rates for reaction equations (5)−(13) are given as[16]

$$r_{\text{devolatilization}} = \varepsilon_p \times 36000 \exp\left(\frac{-9060}{RT_p}\right)\frac{\rho_p Y_{vm}}{MW_{vm}} \tag{14}$$

$$r_{\text{char oxidation}} = \frac{-3\varepsilon_s P_{O_2}}{d_p\left(\frac{1}{k_{film}} + \frac{1}{k_{ash}} + \frac{1}{k_{reaction}}\right)MW_{O_2}} \tag{15}$$

DOI: 10.1021/acs.iecr.6b02506
Ind. Eng. Chem. Res. XXXX, XXX, XXX−XXX

$$r_{\text{steam gasification}} = \alpha_{H_2O} A_{H_2O} \exp\left(\frac{-E_{H_2O}}{RT}\right) \frac{\varepsilon_s \rho_s Y_{\text{char}}}{\text{MW}_{\text{char}}} \frac{{p_{H_2O}}^{n_{H_2O}}}{1 - K_{H_2} p_{H_2}} \quad (16)$$

$$r_{CO_2\ \text{gasification}} = \alpha_{CO_2} A_{CO_2} \exp\left(\frac{-E_{CO_2}}{RT}\right) \frac{\varepsilon_s \rho_s Y_{\text{char}}}{\text{MW}_{\text{char}}} \frac{{p_{CO_2}}^{n_{CO_2}}}{1 - K_{CO} p_{CO}} \quad (17)$$

$$r_{\text{catalytic WGS}} = 9060 \exp\left(-\frac{21700}{RT_g}\right)\left(P_{CO}P_{H_2O} - \frac{P_{H_2}P_{CO_2}}{k_{eq}}\right) \quad (18)$$

$$r_{\text{CO oxidation}} = 1.3 \times 10^{14} \exp\left(-\frac{30000}{RT_g}\right) \varepsilon_g {C_{O_2}}^{0.5} C_{CO} {C_{H_2O}}^{0.5} \quad (19)$$

$$r_{H_2\ \text{oxidation}} = 1.08 \times 10^{16} \exp\left(-\frac{30000}{RT_g}\right) \varepsilon_g C_{O_2} C_{H_2} \quad (20)$$

$$r_{CH_4\ \text{oxidation}} = 1.58 \times 10^{13} \exp\left(-\frac{48400}{RT_g}\right) \varepsilon_g {C_{O_2}}^{0.8} {C_{CH_4}}^{0.7} \quad (21)$$

The shrinking-core gas−solid particle reaction model proposed by Field et al.[17] is used to model char oxidation (i.e., eq 7) . The resistances for the film, ash layer, and surface reactions are defined as

$$k_{\text{film}} = \frac{D_{O_2} Sh}{d_p \frac{R}{\text{MW}_{O_2}} T_g}$$

$$k_{\text{ash}} = \frac{2 r_d D_{\text{eff\_ash}}}{d_p (1 - r_d) \frac{R}{\text{MW}_{O_2}} T_s}$$

$$k_{\text{reaction}} = A_{\text{char oxidation}} \exp\left(-\frac{E_{\text{char oxidation}}}{RT_s}\right) {r_d}^2$$

The other remaining parameters in the rate equations are defined as follows: $A_{\text{char oxidation}}$ = 8710 g/atm·cm^2·s, $E_{\text{char oxidation}}$ = 35700 cal/g·mol, C = molar concentration (kmol/cm^3), d_p = particle diameter, r_s = ratio of the core diameter to the particle diameter $\left[\left(\frac{X^0_{\text{ash}} X_C}{X^0_C X_{\text{ash}}}\right)^{1/3}\right]$, D_{O_2} = oxygen diffusivity $\left[\frac{4.26}{P_{\text{total}}}\left(\frac{T_g}{1800}\right)^{1.75}\right]$, $D_{\text{eff\_ash}}$ = effective ash diffusivity $\{D_{O_2}[0.25 + 0.75(1 - X^0_{\text{ash}})]^{2.5}\}$, P = partial pressure (atm), Sh = Sherwood number $[(7 - 10\varepsilon_g + 5{\varepsilon_g}^2)(1 + 0.7\, Re^{0.2} Sc^{1/3}) + (1.33 - 2.4\varepsilon_g + 1.2\, {\varepsilon_g}^2) Re^{0.7} Sc^{1/3}]$, Sc = Schmidt number, k_{eq} = equilibrium constant for the WGS reaction $(0.0265e^{3956/T_s})$, R = universal gas constant = 1.987 cal/mol·K, T = temperature, α = annealing factor, and ε = volume fraction

Coal devolatilization and gasification reactions are modeled using the computer software *PC Coal Lab* from Niksa Energy Associates LLC.[16] *PC Coal Lab* provides the complete char conversion history of any coal, along with the appropriate molar stoichiometric coefficients and kinetic constants for devolatilization and gasification reaction rates, at user-specified reactor pressure, reactor temperature, and gas composition. Because the local gas composition can vary significantly inside the gasifier, the kinetic constants for the gasification reactions are obtained for a range of gas compositions (CO, CO_2, H_2, and H_2O) at the operating reactor pressure and temperature. The gasification kinetic constants (preexponent, activation energy, order of reaction, and annealing factor) exhibit a strong correlation with the H_2 mole fraction for the range of gas compositions under consideration. Therefore, the kinetic constants in the rate expressions shown by eqs 20 and 21 are expressed as a function of the local H_2 mole fraction in the CFD model. It is noteworthy to add that *PC Coal Lab* recommends calibration of the gasification reaction kinetics by closely matching the actual char conversion history with that predicted by *PC Coal Lab* based on the proximate and ultimate analysis of the coal. However, in this study, because no actual char conversion history was available, we relied on the gasification kinetic constants provided by *PC Coal Lab*, without any further calibration. As such, the kinetic constants for gasification can be treated as an uncertain model input parameter.

The oxidation reaction models of Howard,[18] Peters,[19] and Dryer and Glassman[20] are used to model CO, H_2, and CH_4 oxidation, as shown by eqs 11−13. The catalytic WGS reaction model of Chen et al.[21] (eq 10) is used to account for conversion of CO and steam to H_2 and CO_2 in the presence of coal ash as the catalyst.

Simulation Setup. The bench-scale fluidized-bed gasifier used in this study (as shown in the illustration in Figure 1) consists of a bed section, 0.5 m high with a diameter of 7 cm, and a free board section, 1 m high with a diameter of 15 cm. The cut cell mesh capability in MFiX has been used to construct the Cartesian grid, with a mesh size of 23 × 133 × 23, in x, y, and z directions, respectively. Achieving a grid-independent solution for multiphase flows is quite challenging given the limited computational resources. Hence, to address this important issue, a separate study was initiated to specifically address the effect of the grid resolution,[22] which is briefly discussed under a separate section.

Some of the properties of the fluid and solid phases prescribed during the setup of MFiX simulations are given as follows: the coal particle diameter and coal flow rate were defined based on the corresponding settings from Table 1 for each run (e.g., for baseline cases shown as run 8, the coal particle diameter was 285 μm and the coal flow rate was 0.0495 g/s). An initial coal density of 1100 kg/m^3, with a composition of 41% carbon, 35% volatile matter, 10% moisture, and 14% ash, was prescribed. The second solid phase was defined as sand with a composition of 100% silicon, a particle diameter of 250 μm, a density of 2600 kg/m^3, and an initial temperature of 800 °C.

The gas phase was prescribed as humidified air (19.6% O_2, 16.7% H_2O, and 63.7% N_2) at a rate of 0.189 g/s, and a temperature of 1023.15 K (750 °C) was set to enter into the gasifier. The gasifier operates at atmospheric pressure and a reactor temperature of 1073.15 K (800 °C). In the experiment, the bed temperature was maintained at 1073.15 K by using an electric furnace, which encapsulated the bed section. In order to be able to model the bench-scale fluidized-bed configuration with proper boundary conditions, a new feature that enables a

DOI: 10.1021/acs.iecr.6b02506
Ind. Eng. Chem. Res. XXXX, XXX, XXX−XXX

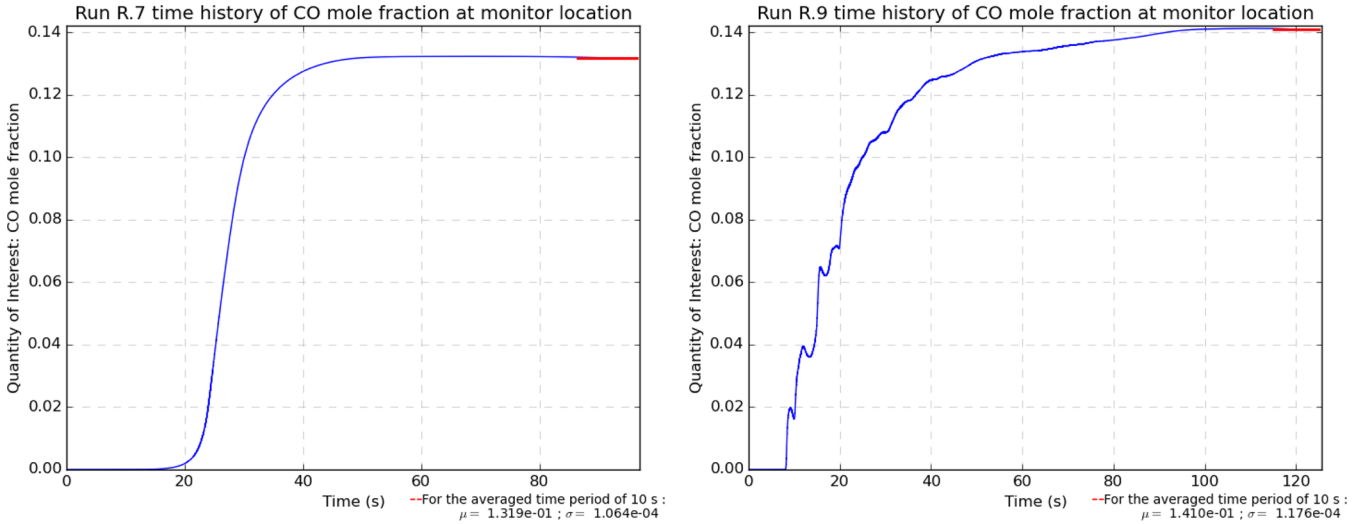

Figure 3. Time history of QoI 1: CO mole fraction for two sampling simulations (R.7 and R.9) showing different convergence characteristics in terms of the simulated time for the simulation campaign with 15 sampling simulations.

point source boundary condition definition was developed and added to MFiX-TFM. No slip boundary conditions have been used for the treatment of gas and solid velocities at the walls instead of partial slip boundary conditions because of the fact that the utilization of partial slip involves the specularity coefficient. Because of the associated uncertainty with the specularity coefficient, ideally one would have to add additional sampling simulations to consider this variable as another uncertain parameter, which would have made the preliminary UQ analysis more costly to perform.

BAYESIAN UQ ANALYSIS OF MFIX SIMULATIONS

In order to perform nonintrusive Bayesian UQ analysis for the CFD simulation results, the same workflow, which was used for the experimental results in Gel et al.[4] was followed using the GEBHM approach. In the current study, in order to replicate the actual physical experiments, initially a CCD-based sampling method was employed in spite of the several shortcomings of the factorial-based sampling approach for GEBHM. Each of the sampling simulations was launched independently and monitored until the determined convergence criteria were reached, which was defined as the "quasi-steady-state" behavior of the time history of the QoIs. The simulation results were then postprocessed and compiled as tabular data, which became input to the GEBHM analysis for the construction of an adequate surrogate model (also known as the emulator) from the sampling simulations performed and for performing UQ analysis such as global sensitivity study.

Sampling CFD Simulations for Nonintrusive UQ Analysis. CFD simulations of reacting multiphase flows are computationally very demanding and require long-duration transient simulations to reach the statistically significant behavior of the QoIs. Hence, for nonintrusive UQ analysis, where a deterministic modeling software is employed for sampling, it is preferred to construct a data-fitted surrogate model that adequately relates the inputs with the QoIs. The surrogate model is then used during UQ analysis instead of the actual CFD simulation. For this purpose, several dedicated simulation campaigns were performed as part of this research effort at NETL. The simulation campaign employed for the purposes of this study basically aimed at replicating the physical experiments by running 3D MFiX simulations with the same set of operating conditions (i.e., coal flow rate, coal particle size, and steam-to-oxygen ratio) and range of values. As discussed earlier, for the physical experiments, a CCD-based sampling approach was employed with 20 samples, where 6 of them were replications of the same operating condition. The transient 3D MFIX simulations employed in the current study are deterministic CFD simulations, which implies that the same results will be obtained when the same operating conditions are simulated. Hence, only 15 samples among the 20 samples were used by eliminating the need to perform any replication runs. The results of the simulation campaign will be presented in this section.

The majority of the simulation campaigns were carried out at the National Energy Research Scientific Computing Center (NERSC) through an award from the 2014 ASCR Leadership Computing Challenge program of the U.S. DOE's Office of Science. The remaining simulations were performed at NETL's High Performance Computing (HPC) system at the Simulation-Based Engineering User Center. The sampling simulations were carried out most of the time concurrently based on the availability of the computing cores on the HPC systems due to the independent nature of the simulations. An MPI-based distributed-memory implementation of MFiX-TFM was employed to achieve a faster time-to-solution. Because of the transient nature of the reacting multiphase flows, each of the sampling simulations was carried out until "quasi-steady state" was reached for the QoIs. Hence, the convergence criteria were based on the assessment for the quasi-steady-state behavior of the QoIs, which were written in a standalone output file at a certain frequency. The time history of the QoIs could be visualized (as illustrated in Figure 3) or statistically analyzed during the progression of the simulations. The QoIs employed in the GEBHM analysis were obtained by taking the time average for the last user-specified duration of simulated time by running a custom Python script, which was developed specifically for this project to handle any number of QoI files under the sampling simulation directories. To ensure that the time-averaging window does not affect the reported QoIs, time averages with several different durations (e.g., for the last 10, 15, and 20 s) were obtained and compared. Figure 3 shows

DOI: 10.1021/acs.iecr.6b02506
Ind. Eng. Chem. Res. XXXX, XXX, XXX−XXX

examples of the time histories from two sampling simulations, and the red line shows the time-averaged value for the last 10 s in each simulation, which is also reported at the lower right corner. As illustrated in Figure 3, each individual simulation reached the quasi-steady state, but after different simulated time durations. For example, run 7 took about 50 s to reach a quasi-steady state, while run 9 took about 120 s of simulated time to reach a quasi-steady state. Hence, this convergence criteria usually resulted in a variability in the total wall clock time required to stop the simulation for each sample under consideration. Such a variability in convergence posed unique challenges as the simulations were conducted in a shared HPC resource with batch-queuing systems and required the generation of several custom workflows to conduct these simulations efficiently. For example, for many high-performance computing sites such as the NERSC, which was employed in the current study, bundling all sampling simulations in a single batch job to request a higher number of cores and longer wall-clock execution time was preferred due to queuing policies in place at the time.

Simulation Campaign with 15 Sampling Simulations Employing the CCD Sampling Method. The target of the first set of simulations was the exact replication of the physical experiments by using the same statistical design of the experiments generating the operating conditions shown in Table 1. Although such a design of experiments matrix is more suited for physical experiments rather than computer experiments, the same run matrix was used for CFD simulations. Hence, 15 distinct MFiX-TFM simulations were set up by changing the three operating variables used in the physical experiments. Because MFiX simulations are deterministic in nature, the six replicated experimental runs for the center point in the CCD sampling method was represented as a single simulation using the same operating conditions. The QoIs were calculated by temporal averaging for the last 10 s of the simulation for each sample.

Effect of the Grid Resolution. A major challenge in the CFD simulation of gas−solid flows is to adequately resolve the structures that exist at different spatial and temporal scales in an inherently transient flow. A rule of thumb for adequate spatial resolution is for the grid spacing to be about 10 times the particle diameter.[23] The grid requirement for maintaining such a ratio of the grid size to the particle diameter for smaller sized particles makes such simulations computationally costly and impractical. Additionally, in reacting gas−solid flow simulations, small time steps are needed in order to not only resolve the temporal scales of the flow but also ensure the numerical stability of the solution. To address the mesh requirements, a series of simulations were carried out at three mesh resolutions, shown in Table 3. The table shows the overall char consumption rate due to steam and CO_2 gasification and char oxidation, along with the time needed for 100 s of simulation time, using 256 computational cores.[22] Although mesh refinement leads to a reduction in char consumption due to the gasification reactions and an increase in char consumption due to char oxidation, observing the rule of thumb of a grid spacing to particle diameter ratio of 10 leads to 209 days of simulation time. The required hardware resources and computational cost make a well-resolved simulation of a reacting gas−solid flow impractical for many CFD practitioners. In the present study, the mesh resolution was set at 70,357 control volumes, which gave about 4 weeks of simulation turnaround time for 100 s of simulation time. With this mesh

Table 3. Mesh Size and Time Requirement for the Simulation of a Bench-Scale Fluidized-Bed Gasifier

	steam-to-oxygen ratio = 1		
mesh resolution (grid spacing/particle diameter)	39375 (35)	315000 (18)	2520000 (9)
char consumption rate for steam gasification (kmol/s)	68.0	63.0	58.1
char consumption rate for char oxidation (kmol/s)	26.5	32.0	37.1
char consumption rate for CO_2 gasification (kmol/s)	5.5	5.0	4.8
time to solution (days)	15	63	209

resolution, it is expected that the uncertainties in the syngas composition shown in the present work include uncertainties due to the discretization error as well, but the current study aimed to study all model discrepancies in an aggregate manner as part of the Bayesian analysis. However, a separate study (Shahnam et al.[22]) was initiated with a focus on determining the effect of the standalone grid resolution.

Simulation Results. The time-averaged mole fraction values for CO and H_2 from MFiX-TFM simulation (green colored solid squares) and measurement from the experiments (red colored asterisks) are shown in Figure 4. Both values of time-averaged CO and H_2 mole fractions are underpredicted at some of the sampling runs and overpredicted at other sampling runs. In order to better quantify the uncertainty in the predicted syngas mole fraction, GEBHM analysis was used to construct emulators for the species mole fraction.

Figure 5 shows the parity plots for the emulator's prediction (y axis) versus experimental results (x axis) for the CO, H_2, and CO_2 mole fractions. Values on the diagonal line indicate perfect agreement between the predictions from the constructed emulator and experiment. The blue solid circles in Figure 5 represent the emulator's prediction of the mole fraction values for the syngas species under consideration at the experiment sampling locations. The intervals represent the uncertainty bands due to propagation of the uncertainties in the three input uncertain parameters (coal flow rate, particle diameter, and steam-to-oxygen ratio). The difference between the solid circle symbols and the diagonal line (actual species mole fraction) is the discrepancy. The red solid squares in Figure 5 are the emulator's prediction after they are corrected for the model discrepancy as part of the GEBHM analysis. Figure 5 shows that the magnitude of the discrepancy varies depending on the values of the uncertain input parameters.

The discrepancy function distributions as a function of the steam-to-oxygen ratio for CO, H_2, and CO_2 mole fractions are shown in Figure 6. A positive value on the y axis of Figure 6 indicates the amount of underprediction in the syngas composition, whereas a negative value on y axis of Figure 6 indicates the amount of overprediction in the syngas composition. The H_2 mole fraction is underpredicted across all operating conditions. The trend observed in the predicted values of the CO mole fraction is changing from under-prediction (at lower steam-tooxygen ratio) to overprediction at higher steam-to-oxygen ratio. The opposite trend is observed in the predicted CO_2 mole fraction behavior.

The response surface plots based on the emulators were constructed with the sampling simulation results obtained from MFiX runs. Figure 7 shows the response surface plots for CO, H_2, and CO_2 mole fractions as a function of the steam-to-oxygen ratio and coal particle size, where the coal flow rate was

DOI: 10.1021/acs.iecr.6b02506
Ind. Eng. Chem. Res. XXXX, XXX, XXX−XXX

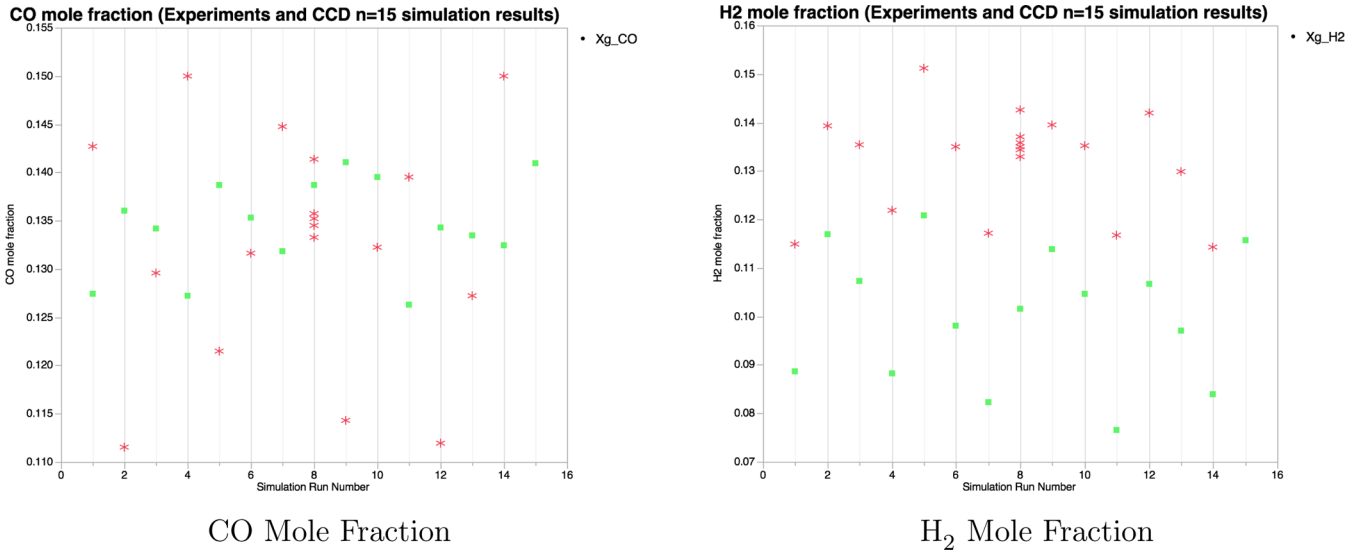

Figure 4. Comparison of the 3D MFiX simulation results for each sampling simulation with respect to the corresponding experimental data (green squares are for 3D MFiX simulations, and red asterisks denote the experiments).

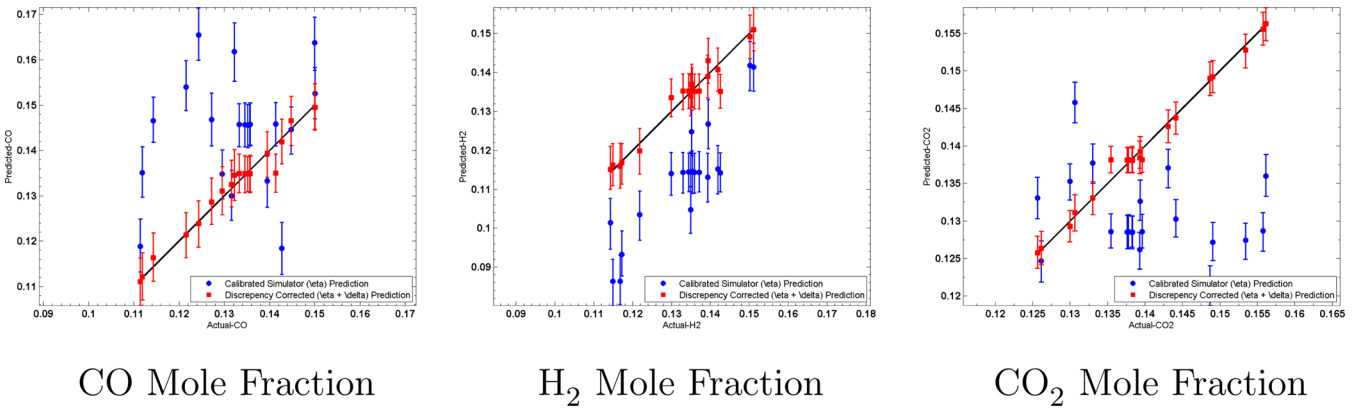

Figure 5. GEBHM surrogate model (emulator) quality for each QoI.

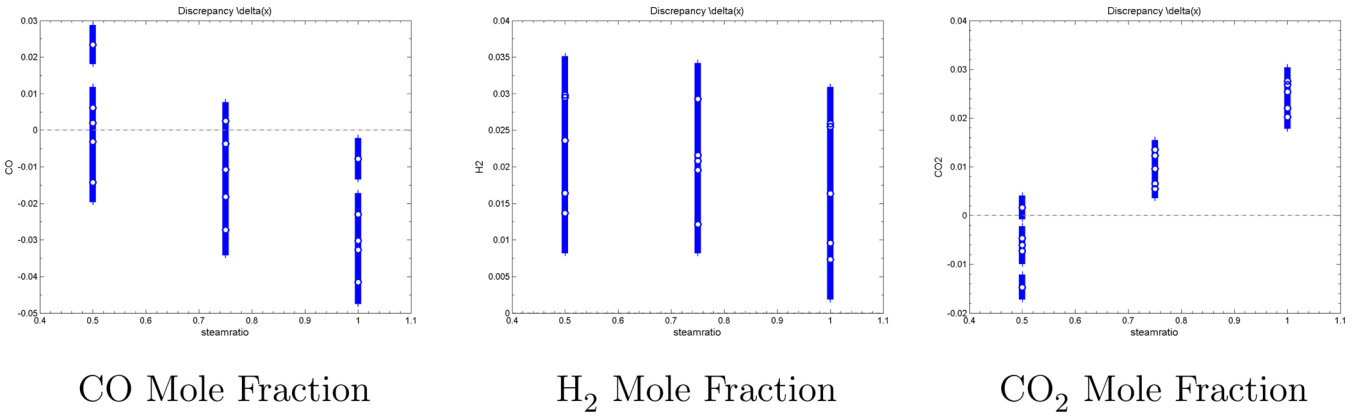

Figure 6. GEBHM discrepancy function distribution.

kept at a nominal setting for illustration purposes. The emulators were constructed based on the GPM in order to establish a model that approximates the relationship between the three input factors and QoIs using the sampling simulation data.

Sensitivity Analysis. The GEBHM analysis employed for the experimental data in an earlier study[4] was replicated for the 3D MFiX simulation results. Hence, Table 4 shows the global sensitivity analysis results for the same QoIs used in the experiment but this time using the MFiX simulation results instead of the standalone experimental data.

Table 4 shows that the variability in the predicted syngas composition is largely due to the coal flow rate for the CO mole fraction, whereas for H_2, it is primarily due to the steam-to-oxygen ratio. The variability in the CO_2 mole fraction, however, is due to all three input parameters. The trends observed in

DOI: 10.1021/acs.iecr.6b02506
Ind. Eng. Chem. Res. XXXX, XXX, XXX−XXX

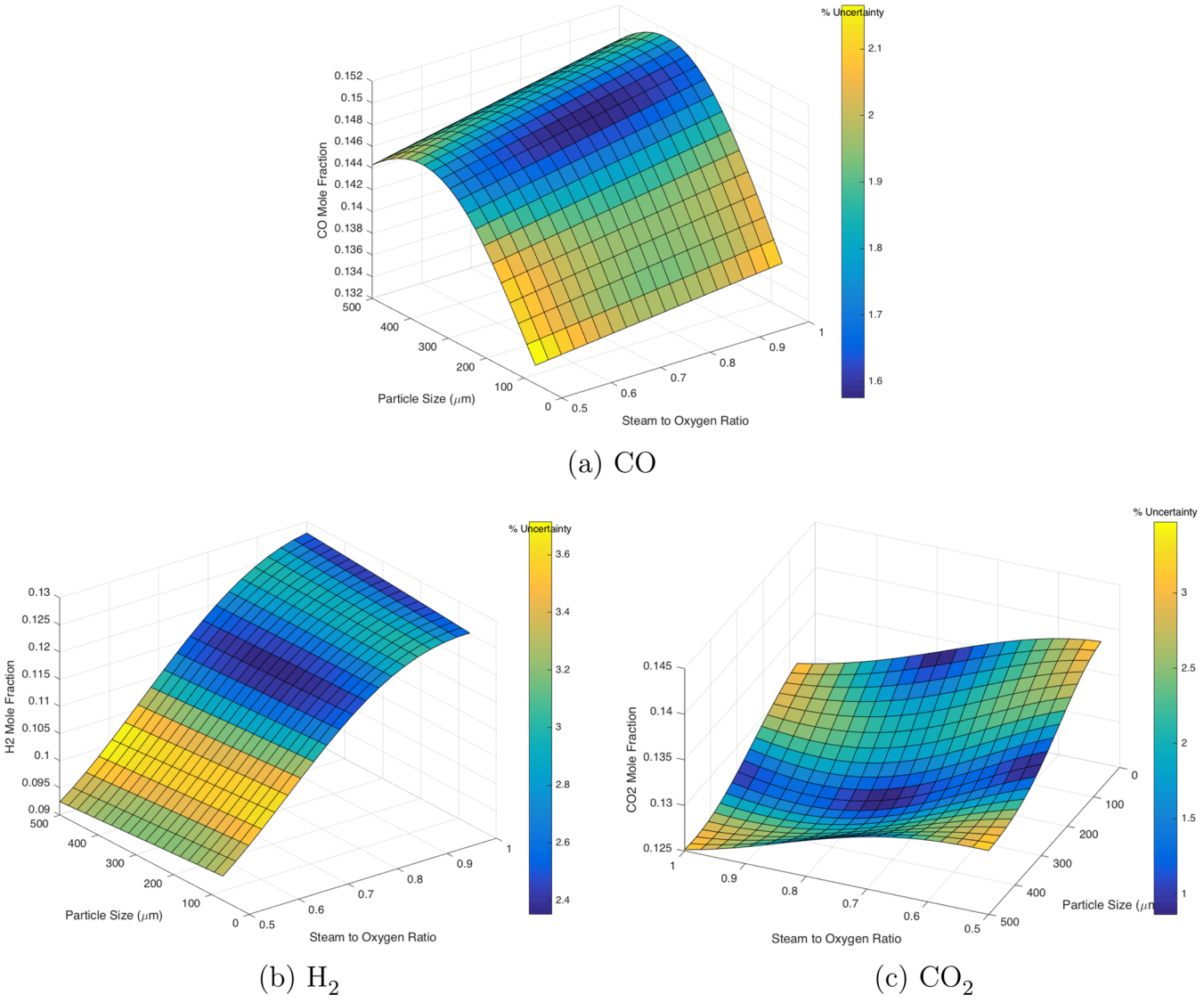

Figure 7. Response surface plot showing the surrogate model (emulator) behavior for QoIs as a function of the steam-to-oxygen ratio and coal particle size (coal flow rate set at the center point), constructed as part of the GEBHM analysis using the 15 MFiX sampling simulation results.

Table 4 are contrary to the trends observed with the experimental data in Table 2, where the steam-to-oxygen ratio was the primary driver for the variability observed in the QoIs.

To further investigate this discrepancy, the sensitivity of CO, H_2, and CO_2 to the variance in each of the primary input parameters (coal flow rate, particle diameter, and steam-to-oxygen ratio) was analyzed utilizing one of the features in the GEBHM analysis, as shown in Figure 8. Unlike what was observed in the experimental data (Figure 2), changes in each of the input parameters affect the mole fraction of CO, H_2, and CO_2. For example, there is a large variance in the sensitivity of CO to the particle flow rate that is caused by the variability in the particle diameter and steam-to-oxygen ratio, or the variance in the sensitivity of CO to the particle diameter is affected by the variability in the coal flow rate and steam-to-oxygen ratio.

The differences observed in the sensitivity analysis of the experimental and predicted syngas compositions indicate that the fluidization behavior may be different in the simulations than in the experiments because the coal flow rate and particle diameter can directly affect the hydrodynamics through a drag force between the gas and solid phases. The effect that the coal flow rate exhibits on the syngas composition can further be observed in Figures 9 and 10. Figure 9 shows the time-averaged reaction rates for the oxidation, char combustion, and char gasification reactions for runs 6 and 10 (refer to Table 1). It is clear that adding more coal to the gasifier (going from run 10 to run 6) leads to an increase in all of the reaction rates. It is also evident that CO oxidation is stronger than char oxidation for both runs 6 and 10. The mole fractions of CO, H_2, and CO_2 (measured and predicted) for runs 6 and 10 are shown in Figure 10, which points to a decrease in the predicted mole fractions of CO and H_2 and an increase in the predicted mole fraction of CO_2 when the coal flow rate into the gasifier increases. On basis of the trends observed in Figures 9 and 10, one can conclude that the extent of homogeneous CO and H_2 oxidation reactions in the bed is greater than the extent of heterogeneous reactions taking place when the coal flow rate is increased. Additionally, Table 4 and Figure 8 show that the CO mole fraction is not sensitive to the steam-to-oxygen ratio. This indicates that, in simulation, the coal combustion reaction is not greatly affected by increasing or decreasing the oxygen flow into

DOI: 10.1021/acs.iecr.6b02506
Ind. Eng. Chem. Res. XXXX, XXX, XXX−XXX

Table 4. Global Sensitivity of the QoIs with Respect to the Operating Variables Based on 3D MFiX Simulations with CCD Sampling

% Contribution to the Variability Seen in the CO Mole Fraction			
	factor 1	factor 2	factor 3
	CF	PS	H_2O/O_2
CF: coal flow rate (g/s)	**84.7**	0.57	0.0
PS: particle size (μm)		14.1	0.0
H_2O/O_2 ratio in syngas			0.6
% Contribution to the Variability Seen in the H_2 Mole Fraction			
	factor 1	factor 2	factor 3
	CF	PS	H_2O/O_2
CF: coal flow rate (g/s)	26.7	0.02	1.2
PS: particle size (μm)		0.1	0.1
H_2O/O_2 ratio in syngas			**71.9**
% Contribution to the Variability Seen in the CO_2 Mole Fraction			
	factor 1	factor 2	factor 3
	CF	PS	H_2O/O_2
CF: coal flow rate (g/s)	**36.5**	2.11	3.1
PS: particle size (μm)		27.9	2.1
H_2O/O_2 ratio in syngas			27.6

the gasifier. Therefore, the fluidization and mixing behavior in the experiment have to be somewhat different from the hydrodynamic behavior that the model is predicting.

DISCUSSION

The steam-to-oxygen ratio is the primary uncertain input parameter affecting the variability of the syngas composition in the experiments, as shown in Karimipour et al.[9] and Gel et al.[4] Although in the experiments the syngas composition does not show any sensitivity toward the particle flow rate and particle diameter directly, these two factors affect the sensitivity that the syngas composition shows toward the steam-to-oxygen ratio.[4] Because steam and oxygen are oxidizers to the char in coal, the steam-to-oxygen ratio can be thought of as an input parameter, which can directly affect the kinetics of the combustion, gasification, and, in turn, WGS reactions. On the other hand, the particle flow rate and particle diameter are input parameters that influence the hydrodynamics of the fluidized bed. The drag between the gas and solid phases is directly affected by the particle diameter. Any increase or decrease in the drag between the gas and solid phases can modify the coal particle distribution throughout the reacting bed.

The global sensitivity analysis of the simulation results shows that the predicted syngas composition is strongly affected not only by the steam-to-oxygen ratio (influencing the reaction kinetics) but also by variation in the coal flow rate and particle diameter (influencing the hydrodynamics). Moreover, the interaction between each of the three uncertain input parameters also affects the variability in the predicted syngas composition. In particular, the variance in each of the input parameters affects the uncertainty in the syngas composition due to the other two input parameters.

Such differences in the sensitivity analysis result between the experimental and CFD-simulation-predicted syngas composition values point to the need for modeling improvement in both the hydrodynamic and kinetic areas such as the following:

(1) Improvements in the fluidization behavior, mixing, and segregation between the phases that could lead to a reduction in the sensitivity of the syngas composition to hydrodynamic effects. This may be done through the use of other drag models for the gas/solid and solid/solid phases for the particle range considered in this study (70, 250, and 500 μm). Alternatively, improvements in the modeling capabilities to account for clustering of the solid particles could lead to a reduction in the drag between the gas and solid phases. Figure 11 shows the time-averaged coal and sand volume fractions for one of the test conditions. The lighter coal particles are expected to segregate from the denser sand particles. However, because no visual information is available on how mixed or segregated the fluidized bed is in the experiment, the degree to which coal and sand particle segregation is taking place in the simulations deserves a closer look. Additionally, the effect of the grid resolution on the syngas composition will have to be examined, which was initiated as a separate study[22] based on the findings of the current study.

(2) Different reaction models or reaction kinetics for the gasification, char and gaseous oxidation, and WGS reactions. Figure 12 shows the relationship between CO, H_2, and CO_2 for both the measured and predicted values at each sampling point. The ellipse representation in the figure shows the region enclosing approximately 95% of the sampling points if the variables were assumed to be bivariate normally distributed. Hence, if the ellipse appears as fairly narrow and diagonally oriented, then there is a strong correlation between the two variables (e.g., CO and CO_2 mole fractions in the experimental data). If the ellipse appears to be round and not diagonally oriented, then the variables are considered to be uncorrelated. The experimental data show that, as the steam-to-oxygen ratio increases, the overall trend in the gasifier is an increase in the CO_2 mole fraction and a decrease in the CO mole fraction. However, the opposite trend is observed in the predicted results. This difference points to the need for improvements in reaction models such as gasification, oxidation, and WGS

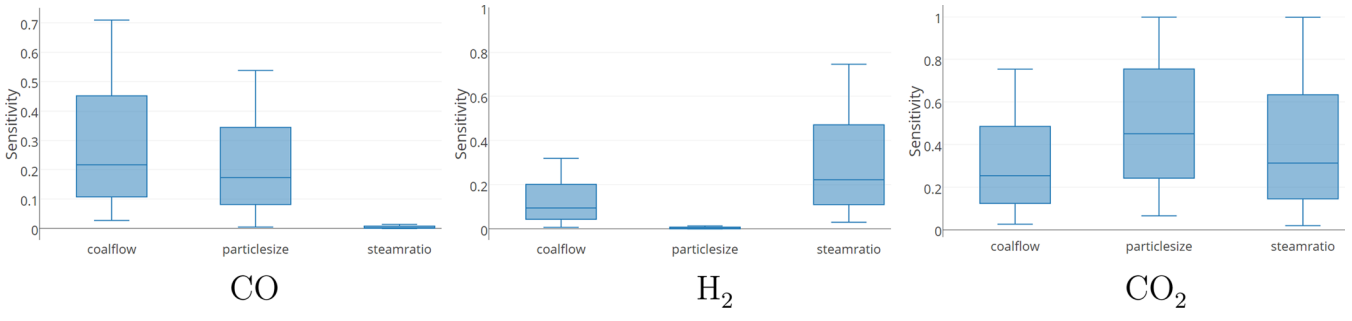

Figure 8. Variance of the global sensitivity for each QoI based on the MFiX simulation results.

DOI: 10.1021/acs.iecr.6b02506
Ind. Eng. Chem. Res. XXXX, XXX, XXX−XXX

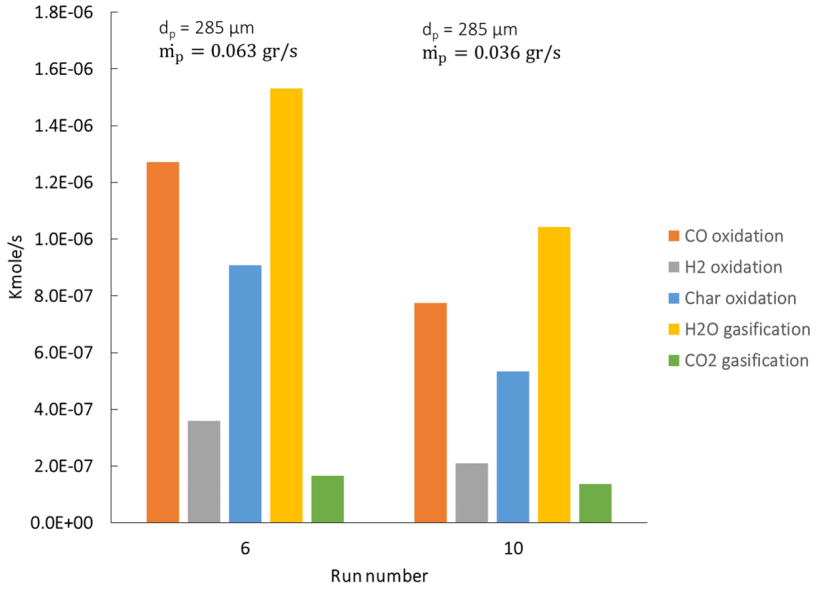

Figure 9. Time-averaged predicted reaction rates for runs 6 and 10.

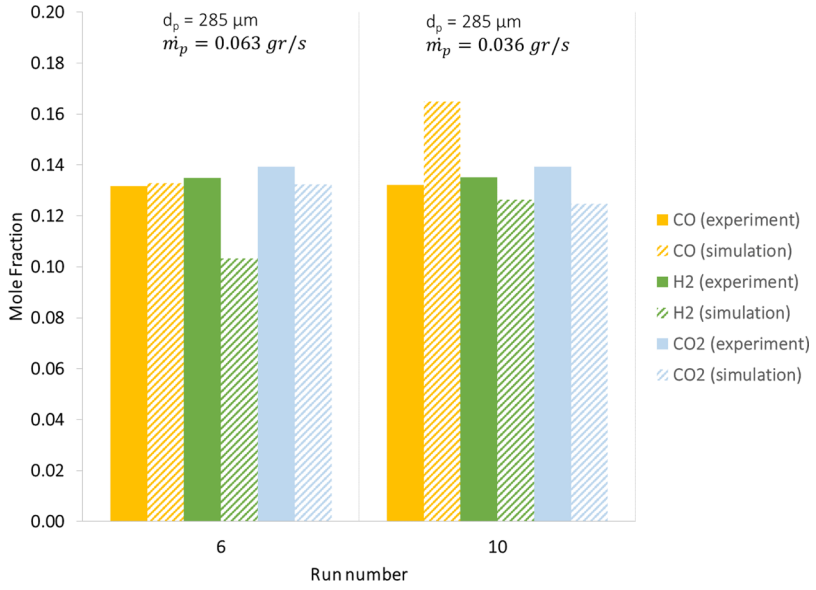

Figure 10. Comparison between the CO and H_2 compositions for runs 6 and 10, both predicted and measured.

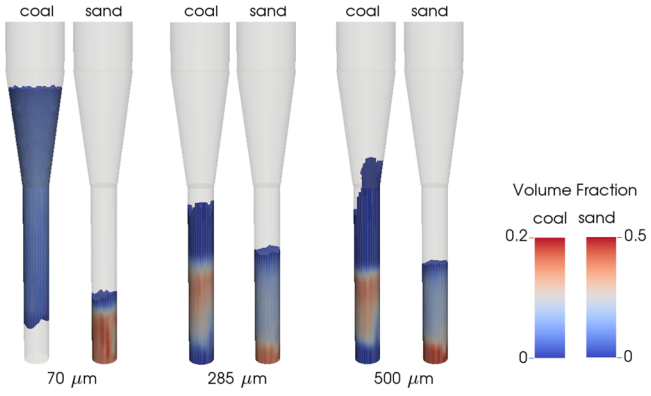

Figure 11. Time-averaged volume fractions of coal and sand, for coal particle diameters of 70 μm (left), 285 μm (center), and 500 μm (right).

because all of these reactions lead to the production of CO, CO_2, and H_2. In particular, the WGS reaction converts CO and steam to H_2 and CO_2.

CONCLUSIONS

The global sensitivity analysis shows that the predicted syngas composition is strongly affected not only by the steam-to-oxygen ratio (which was observed in the experiments as well) but also by variation in the coal flow rate and particle diameter (which was not observed in the experiments). The CO mole fraction is underpredicted at lower steam-to-oxygen ratios and overpredicted at higher steam-to-oxygen ratios. The opposite trend is observed for the CO_2 mole fraction. These discrepancies are attributed to either (i) excessive segregation of the phases, which leads to the fuel-rich or -lean regions, where homogeneous and heterogeneous reactions can over- or underproduce the product gases, or (ii) selection of the reaction models, where different reaction models and kinetics

DOI: 10.1021/acs.iecr.6b02506
Ind. Eng. Chem. Res. XXXX, XXX, XXX−XXX

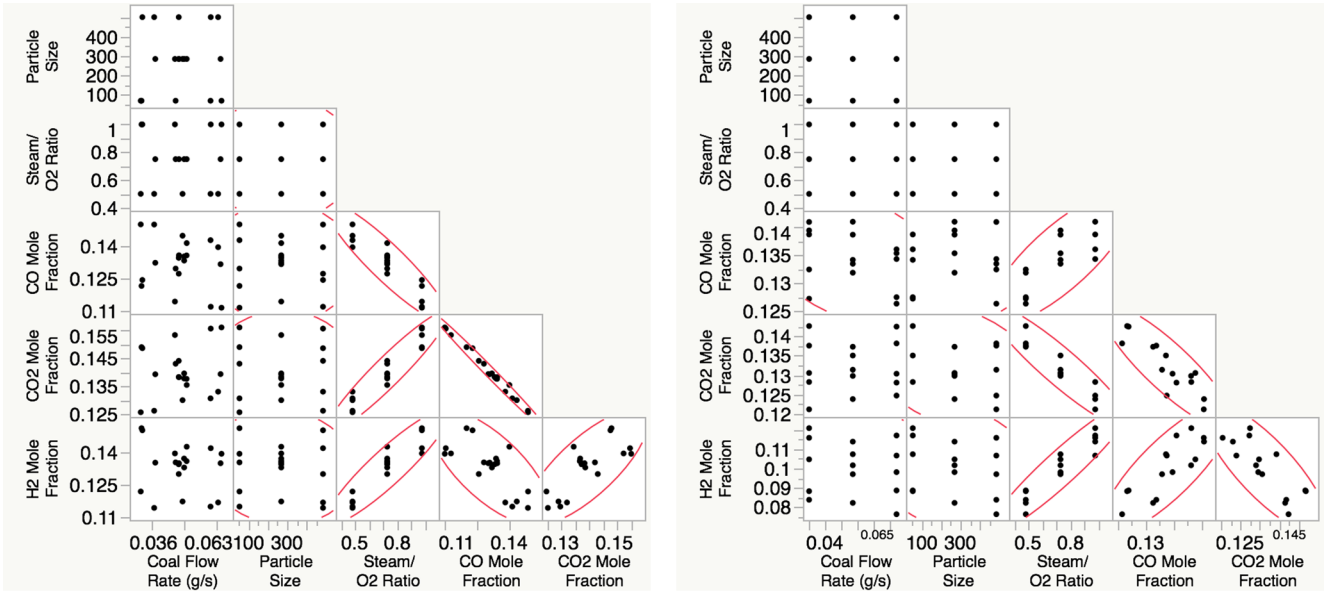

Figure 12. Scatter plot of the experimental data and 3D MFiX simulation results for same set of operating conditions based on CCD sampling.

can lead to different syngas compositions throughout the gasifier. Work is underway to investigate each of these factors, i.e., the effect of gasification, char combustion, CO oxidation, and WGS reactions, along with the bed temperature and grid resolution, on the syngas composition.

AUTHOR INFORMATION

Corresponding Author

*E-mail: aike@alpemi.com.

Notes

This project was funded by the U.S. DOE, NETL, an agency of the United States Government, through a support contract with AECOM. Neither the United States Government nor any agency thereof, nor any of their employees, nor AECOM, nor any of their employees, makes any warranty, expressed or implied, or assumes any legal liability or responsibility for the accuracy, completeness, or usefulness of any information, apparatus, product, or process disclosed, or represents that its use would not infringe privately owned rights. Reference herein to any specific commercial product, process, or service by trade name, trademark, manufacturer, or otherwise, does not necessarily constitute or imply its endorsement, recommendation, or favoring by the United States Government or any agency thereof. The views and opinions of authors expressed herein do not necessarily state or reflect those of the United States Government or any agency thereof.

The authors declare no competing financial interest.

ACKNOWLEDGMENTS

This technical effort was performed in support of NETL ongoing research under the RES Contract DE-FE0004000. The work presented is a joint effort between NETL and GE Global Research Center performed under a cooperative research and development agreement (No. AGMT-0407). The authors thank and acknowledge that this research used resources allocated through the 2014 ASCR Leadership Computing Challenge (ALCC) program at the NERSC, a U.S. DOE Office of Science User Facility supported by the Office of Science of the U.S. DOE under Contract DE-AC02-05CH11231.

REFERENCES

(1) Gel, A.; Li, T.; Gopalan, B.; Shahnam, M.; Syamlal, M. *Ind. Eng. Chem. Res.* **2013**, *52*, 11424−11435.

(2) Gel, A.; Garg, R.; Tong, C.; Shahnam, M.; Guenther, C. *Powder Technol.* **2013**, *242*, 27−39.

(3) Roy, C. J.; Oberkampf, W. L. *Computer Methods in Applied Mechanics and Engineering* **2011**, *200*, 2131−2144.

(4) Gel, A.; Shahnam, M.; Subramaniyan, A. K. *Powder Technology* **2016**.

(5) Kennedy, M. C.; O'Hagan, A. *Journal of the Royal Statistical Society: Series B (Statistical Methodology)* **2001**, *63*, 425−464.

(6) Subramaniyan, A. K.; Wang, L.; Beeson, D.; Nelson, J.; Berg, R.; Cepress, R. A Comparative Study on Accuracy and Efficiency of Metamodels for Large Industrial Datasets. *ASME Turbo Expo: Turbine Technical Conference and Exposition*; 2011; pp 759−769.

(7) Subramaniyan, A. K.; Kumar, N. C.; Wang, L. Probabilistic Validation of Complex Engineering Simulations with Sparse Data. *ASME Turbo Expo: Turbine Technical Conference and Exposition*, 2014; pp V07BT30A003−V07BT30A003.

(8) Kumar, N. C.; Subramaniyan, A. K.; Wang, L. Improving high-dimensional physics models through Bayesian calibration with uncertain data. *ASME Turbo Expo: Turbine Technical Conference and Exposition*, 2012; pp 407−416.

(9) Karimipour, S.; Gerspacher, R.; Gupta, R.; Spiteri, R. J. *Fuel* **2013**, *103*, 308−320.

(10) Karimipour, S. Personal Communication, Calgary, Canada, 2013

(11) Myers, R. H.; Montgomery, D. C.; Anderson-Cook, C. M. *Response surface methodology: process and product optimization using designed experiments*; John Wiley & Sons: New York, 2009; Vol. *705*.

(12) Holloway, J. P.; Bingham, D. C.; Chou, C.-C.; Doss, F.; Drake, R. P.; Fryxell, B.; Grosskopf, M.; Van der Holst, B.; Mallick, B. K.; McClarren, R.; Mukherjee, A.; Nair, V.; Powell, K. G.; Ryu, D.; Sokolov, I.; Toth, G.; Zhang, Z. *Reliability Engineering & System Safety* **2011**, *96*, 1184−1193.

(13) National Energy Technology Laboratory (NETL) Multiphase Flow Science Website, Multiphase Flow with Interphase eXchanges (MFIX). 2016, https://mfix.netl.doe.gov/mfix/mfix-documentation/.

(14) Syamlal, M.; Rogers, W.; O'Brien, T. J. MFIX Documentation Theory Guide. https://mfix.netl.doe.gov/documentation/Theory.pdf.

DOI: 10.1021/acs.iecr.6b02506
Ind. Eng. Chem. Res. XXXX, XXX, XXX−XXX

(15) Benyahia, S.; Syamlal, M.; O'Brien, T. J. Summary of MFIX Equations 2012-1. https://mfix.netl.doe.gov/documentation/MFIXEquations2012-1.pdf.
(16) Niksa, S. *PC Coal Lab version 4.1: user guide and tutorial*; Niksa Energy Associates LLC: Belmont, CA, 1997.
(17) Field, M.; Gill, D.; Morgan, B.; Hawksley, P. *Combustion of Pulverized Coal*; British Coal Utilisation Research Association: Leatherhead, England, 1967.
(18) Howard, J. B. *Chemistry of coal utilization*, Second Supplementary Volume, Wiley: New York, 1981; pp 625−784.
(19) Peters, N. *Int. J. Heat Mass Transfer* **1979**, *22*, 691−703.
(20) Dryer, F.; Glassman, I. High Temperature Oxidation of CO and CH_4; *14th Symposium (International) on Combustion*. Pittsburgh, The Combustion Institute, pp 978−1003, 1973.
(21) Chen, W.; Sheu, F.; Savage, R. *Fuel Process. Technol.* **1987**, *16*, 279−288.
(22) Shahnam, M.; Gel, A.; Dietiker, J.-F.; Subramaniyan, A. K.; Musser, J. *J. Verification, Validation Uncertainty Quantification* **2016**.
(23) Pannala, S. *Computational Gas−Solids Flows and Reacting Systems: Theory, Methods and Practice*; IGI Global: Hershey, PA, 2010.

DOI: 10.1021/acs.iecr.6b02506
Ind. Eng. Chem. Res. XXXX, XXX, XXX−XXX